






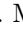

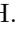





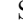

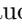

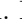
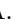





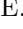





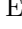







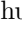
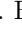
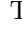



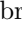




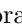






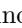


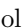


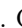


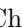














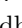



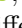
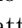




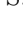


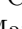
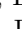
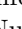
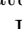







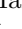
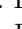

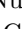
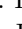

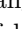




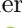
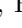
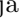

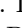

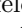



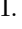


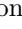
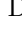






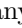



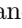
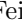













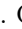









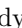



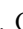
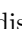


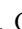


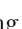





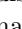


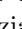


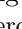
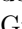










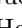





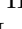


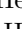


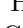
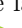
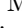
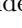

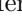





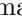




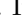



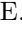
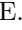



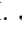
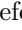









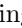














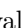


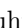
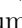





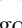
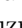


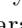







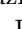
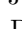


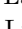
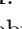

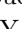




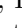
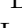
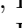
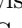




















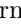

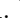

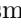
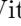
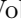



February 24, 2023

Measurement of the B^0 lifetime and flavor-oscillation frequency using hadronic decays reconstructed in 2019-2021 Belle II data

F. Abudinén , I. Adachi , L. Aggarwal , H. Ahmed , H. Aihara , N. Akopov , A. Aloisio , N. Anh Ky , D. M. Asner , H. Atmacan , T. Aushev , V. Aushev , H. Bae , S. Bahinipati , P. Bambade , Sw. Banerjee , S. Bansal , M. Barrett , J. Baudot , M. Bauer , A. Baur , A. Beaubien , J. Becker , J. V. Bennett , E. Bernieri , F. U. Bernlochner , V. Bertacchi , M. Bertemes , E. Bertholet , M. Bessner , S. Bettarini , V. Bhardwaj , B. Bhuyan , F. Bianchi , T. Bilka , S. Bilokin , D. Biswas , A. Bobrov , D. Bodrov , J. Borah , A. Bozek , M. Bračko , R. A. Briere , T. E. Browder , A. Budano , S. Bussino , M. Campajola , L. Cao , G. Casarosa , C. Cecchi , J. Cerasoli , P. Chang , P. Cheema , V. Chekelian

, C. Chen , B. G. Cheon , K. Chilikin , K. Chirapatpimol , H.-E. Cho , K. Cho , S.-J. Cho , S.-K. Choi , S. Choudhury , J. Cochran , L. Corona , S. Cunliffe , F. Dattola , E. De La Cruz-Burelo , S. A. De La Motte , G. de Marino , G. De Nardo , M. De Nuccio , G. De Pietro , R. de Sangro , M. Destefanis , A. De Yta-Hernandez , R. Dhamija , A. Di Canto , F. Di Capua , J. Dingfelder , Z. Doležal , I. Domínguez Jiménez , T. V. Dong , M. Dorigo , K. Dort , D. Dossett , S. Dreyer , S. Dubey , G. Dujany , P. Ecker , M. Eliachevitch , D. Epifanov , P. Feichtinger , T. Ferber , D. Ferlewicz , T. Fillingner , G. Finocchiaro , A. Fodor , F. Forti , A. Frey , B. G. Fulsom , A. Gabrielli , E. Ganiev , M. Garcia-Hernandez , G. Gaudino , V. Gaur , A. Gaz

, A. Gellrich , G. Ghevondyan , D. Ghosh , G. Giakoustidis , R. Giordano , A. Giri , A. Glazov , B. Gobbo , R. Godang , P. Goldenzweig , W. Gradl , T. Grammatico , S. Granderath , E. Graziani , D. Greenwald , Z. Gruberová , T. Gu , K. Gudkova , S. Halder , K. Hara , T. Hara , K. Hayasaka , H. Hayashii , S. Hazra , C. Hearty , M. T. Hedges , I. Heredia de la Cruz , M. Hernández Villanueva , A. Hershenhorn , T. Higuchi , E. C. Hill , M. Hohmann , C.-L. Hsu , T. Humair , T. Iijima , K. Inami , N. Ipsita , A. Ishikawa , S. Ito , R. Itoh , M. Iwasaki , W. W. Jacobs , D. E. Jaffe , E.-J. Jang , Q. P. Ji , S. Jia , Y. Jin , H. Junkerkalefeld , M. Kaleta , A. B. Kaliyar , K. H. Kang , G. Karyan , T. Kawasaki , C. Kiesling

, C.-H. Kim , D. Y. Kim , K.-H. Kim , Y.-K. Kim , H. Kindo , P. Kodyš , T. Koga , S. Kohani , K. Kojima , A. Korobov , S. Korpar , E. Kovalenko , R. Kowalewski , P. Križan , P. Krokovny , T. Kuhr , J. Kumar , R. Kumar , K. Kumara , T. Kunigo , A. Kuzmin , Y.-J. Kwon , S. Lacaprrara , J. S. Lange , M. Laurenza , R. Leboucher , F. R. Le Diberder , P. Leitl , D. Levit , P. M. Lewis , L. K. Li , J. Libby , Z. Liptak , Q. Y. Liu , Z. Q. Liu , D. Liventsev , S. Longo , T. Lueck , C. Lyu , Y. Ma , M. Maggiora , S. P. Maharana , R. Maiti , S. Maity , R. Manfredi , E. Manoni , A. C. Manthai , M. Mantovano , D. Marcantonio , S. Marcello , C. Marinas , L. Martel , C. Martellini , A. Martini

, T. Martinov , L. Massaccesi , M. Masuda , K. Matsuoka , D. Matvienko , S. K. Maurya , J. A. McKenna , F. Meier , M. Merola , F. Metzner , M. Milesi , C. Miller , K. Miyabayashi , H. Miyake , R. Mizuk , G. B. Mohanty , N. Molina-Gonzalez , S. Moneta , H.-G. Moser , M. Mrvar , R. Mussa , I. Nakamura , K. R. Nakamura , M. Nakao , Y. Nakazawa , A. Narimani Charan , M. Naruki , D. Narwal , A. Natochii , L. Nayak , G. Nazaryan , C. Niebuhr , N. K. Nisar , S. Nishida , S. Ogawa , H. Ono , Y. Onuki , P. Oskin , P. Pakhlov , G. Pakhlova , A. Paladino , A. Panta , S. Pardi , K. Parham , J. Park , S.-H. Park , B. Paschen , A. Passeri , S. Patra , S. Paul , T. K. Pedlar , I. Peruzzi , R. Peschke , R. Pestotnik

, F. Pham , L. E. Piilonen , G. Pinna Angioni , P. L. M. Podesta-Lerma , T. Podobnik , S. Pokharel , L. Polat , C. Praz , S. Prell , E. Prencipe , M. T. Prim , H. Purwar , N. Rad , P. Rados , G. Raeuber , S. Raiz , M. Reif , S. Reiter , I. Ripp-Baudot , G. Rizzo , L. B. Rizzuto , J. M. Roney , A. Rostomyan , N. Rout , Y. Sakai , D. A. Sanders , S. Sandilya , A. Sangal , L. Santelj , Y. Sato , B. Scavino , C. Schmitt , C. Schwanda , A. J. Schwartz , Y. Seino , A. Selce , K. Senyo , J. Serrano , M. E. Sevir , C. Sfienti , W. Shan , C. Sharma , C. P. Shen , T. Shillington , J.-G. Shiu , D. Shtol , F. Simon , J. B. Singh , J. Skorupa , R. J. Sobie , A. Soffer , E. Solovieva , S. Spataro , B. Spruck

, M. Starič , S. Stefkova , R. Stroili , Y. Sue , M. Sumihama , W. Sutcliffe , S. Y. Suzuki , H. Svidras , M. Takahashi , M. Takizawa , U. Tamponi , S. Tanaka , K. Tanida , H. Tanigawa , N. Taniguchi , F. Tenchini 

R. Tiwary , D. Tonelli , E. Torassa , K. Trabelsi , I. Tsaklidis , M. Uchida , I. Ueda , Y. Uematsu ,
T. Uglov , K. Unger , Y. Unno , K. Uno , S. Uno , P. Urquijo , Y. Ushiroda , S. E. Vahsen ,
R. van Tonder , G. S. Varner , K. E. Varvell , A. Vinokurova , V. S. Vismaya , L. Vitale , V. Vobbilisetti ,
A. Vossen , M. Wakai , H. M. Wakeling , S. Wallner , E. Wang , M.-Z. Wang , X. L. Wang , Z. Wang ,
A. Warburton , M. Watanabe , S. Watanuki , M. Welsch , C. Wessel , E. Won , X. P. Xu , B. D. Yabsley ,
S. Yamada , W. Yan , S. B. Yang , H. Ye , J. Yelton , J. H. Yin , Y. M. Yook , K. Yoshihara , Y. Yusa ,
L. Zani , Y. Zhai , Y. Zhang , V. Zhilich , Q. D. Zhou , X. Y. Zhou , V. I. Zhukova , and R. Žlebčik

(The Belle II Collaboration)

We measure the B^0 lifetime and flavor-oscillation frequency using $B^0 \rightarrow D^{(*)-}\pi^+$ decays collected by the Belle II experiment in asymmetric-energy e^+e^- collisions produced by the SuperKEKB collider operating at the $\Upsilon(4S)$ resonance. We fit the decay-time distribution of signal decays, where the initial flavor is determined by identifying the flavor of the other B meson in the event. The results, based on 33000 signal decays reconstructed in a data sample corresponding to 190 fb^{-1} , are

$$\begin{aligned}\tau_{B^0} &= (1.499 \pm 0.013 \pm 0.008) \text{ ps} \\ \Delta m_d &= (0.516 \pm 0.008 \pm 0.005) \text{ ps}^{-1},\end{aligned}$$

where the first uncertainties are statistical and the second are systematic. These results are consistent with the world-average values.

Knowledge of the B^0 lifetime τ_{B^0} , and the flavor-oscillation frequency Δm_d , allows us to test both the QCD theory of strong interactions at low energy and the Cabibbo-Kobayashi-Maskawa (CKM) theory of weak interactions [1, 2]. The Belle, Babar, and LHCb collaborations have measured τ_{B^0} and Δm_d to comparable precision [3–6]. Additionally, the CMS, ATLAS, D0 and CDF collaborations have measured τ_{B^0} to similar precision [7–10]. LHCb’s measurements, $\tau_{B^0} = (1.524 \pm 0.006 \pm 0.004) \text{ ps}$ and $\Delta m_d = (0.5050 \pm 0.0021 \pm 0.0010) \text{ ps}^{-1}$, are the most precise to-date [5, 6],[11] When two uncertainties are given, the first is statistical and the second is systematic.

Here we report a new measurement of τ_{B^0} and Δm_d using hadronic decays of B^0 mesons reconstructed in a 190 fb^{-1} data set collected by the Belle II experiment at the SuperKEKB asymmetric-energy e^+e^- collider. The data were collected between 2019 and 2021. The B^0 mesons are produced in the $e^+e^- \rightarrow \Upsilon(4S) \rightarrow B\bar{B}$ process, where B indicates a B^0 or a B^+ . Our data set contains approximately 200 million such events. Our measurement tests the ability of Belle II to precisely measure B^0 meson decay times and also identify the initial flavor of the decaying B^0 ; such capabilities are crucial for measuring decay-time-dependent CP violation and determining ϕ_1 and ϕ_2 , two of the three angles of the B^0 CKM unitarity triangle.[12] Examples of measurements of ϕ_1 and ϕ_2 are found in Refs. [13, 14].

The flavor of a neutral B^0 or \bar{B}^0 meson oscillates with frequency Δm_d before it decays. The probability density of a B initially being in a particular flavor state and decaying after time Δt in the same flavor state ($q_f = +1$)

or in the opposite flavor state ($q_f = -1$) is

$$P(\Delta t, q_f | \tau_{B^0}, \Delta m_d) = \frac{e^{-|\Delta t|/\tau_{B^0}}}{4\tau_{B^0}} [1 + q_f \cos(\Delta m_d \Delta t)]. \quad (1)$$

By measuring the distribution of Δt and q_f , we determine both τ_{B^0} and Δm_d . In each event, we fully reconstruct the “signal-side” B (B_{sig}) via $B^0 \rightarrow D^{(*)-}\pi^+$ decays, identifying its flavor via the pion charge, as the contribution from $\bar{B}^0 \rightarrow D^{(*)-}\pi^+$ decays is of the order of 10^{-4} [15–18] and hence can be neglected here. Throughout this paper, charge-conjugate modes are implicitly included unless stated otherwise.

We use a flavor-tagging algorithm to determine the flavor of the other, or “tag-side”, B meson (B_{tag}) when it decays [19]. As the B mesons are produced in a quantum-entangled state, the flavor of B_{tag} when it decays identifies (or tags) the flavor of B_{sig} at that instant [20, 21]. From that time onwards, the signal-side B freely oscillates in flavor. The variable Δt is the difference between the proper decay times of the B_{sig} and B_{tag} . Equation 1 also applies when B_{sig} decays first, *i.e.*, for negative Δt .

At SuperKEKB [22], the $\Upsilon(4S)$ is produced with a Lorentz boost in the laboratory frame of $\beta\gamma = 0.28$. Since the B mesons are nearly at rest in the $\Upsilon(4S)$ rest frame, their momenta are mostly determined by the $\Upsilon(4S)$ boost, resulting in a mean displacement between the B_{sig} and B_{tag} decay positions of the order of $100\text{ }\mu\text{m}$ along the boost direction. By measuring the relative displacement, and knowing the $\Upsilon(4S)$ boost, we determine Δt . To measure τ_{B^0} and Δm_d , we fit Eq. (1), modified to account for the B_{tag} decay probability and detection effects, to the background-subtracted Δt distribution.

The Belle II detector consists of subsystems arranged cylindrically around the interaction region [23]. The z

axis of the laboratory frame is defined as the symmetry axis of the cylinder, and the positive direction is approximately given by the electron-beam direction, which is the beam with higher energy. The polar angle θ , as well as the longitudinal and transverse directions, are defined with respect to the $+z$ axis. Charged-particle trajectories (tracks) are reconstructed by a two-layer silicon-pixel detector (PXD) surrounded by a four-layer double-sided silicon-strip detector (SVD) and a 56-layer central drift chamber (CDC). When the data analyzed here were collected, only one sixth of the second PXD layer was installed. A quartz-based Cherenkov counter measuring the Cherenkov photon time-of-propagation is used to identify hadrons in the central region, and an aerogel-based ring-imaging Cherenkov counter is used to identify hadrons in the forward end-cap region. An electromagnetic calorimeter (ECL) is used to reconstruct photons and to provide information for particle identification, in particular, to distinguish electrons from other charged particles. All subsystems up to the ECL are located within an axially uniform 1.5 T magnetic field provided by a superconducting solenoid. A subsystem dedicated to identifying K_L^0 mesons and muons is the outermost part of the detector.

The data is processed with the Belle II analysis software framework [24] using the track reconstruction algorithm described in Ref. [25]. We use Monte Carlo (MC) simulation to optimize selection criteria, determine shapes of probability density functions (PDFs), and study sources of background. We use KKMC [26] to generate $e^+e^- \rightarrow q\bar{q}$, where q indicates a u , d , c , or s quark, PYTHIA8 [27] to simulate hadronization, EVTGEN [28] to simulate decays of hadrons, and GEANT4 [29] to model detector response. Our simulation includes beam-induced backgrounds [30]. We optimize and fix our selection criteria using simulated data before examining the experimental data.

We reconstruct $B^0 \rightarrow D^{*-}\pi^+$ and $B^0 \rightarrow D^-\pi^+$ decays by first reconstructing D mesons via $D^- \rightarrow K^+\pi^-\pi^-$, $\bar{D}^0 \rightarrow K^+\pi^-$, $\bar{D}^0 \rightarrow K^+\pi^-\pi^0$, and $\bar{D}^0 \rightarrow K^+\pi^-\pi^+\pi^-$ decays. We then reconstruct D^{*-} mesons in their decay to a $\bar{D}^0\pi^-$ final state, where the pion is referred to as the “slow pion”—one with low momentum in the $\Upsilon(4S)$ rest frame. Finally, we combine a D^- or D^{*-} candidate with a charged particle identified as a pion to form the B^0 candidate.

We require that tracks originate from the interaction region and have at least six measurement points (hits) in the SVD or twenty hits in the CDC. Each track must have a distance-of-closest-approach to the interaction point of less than 3 cm along the z axis and less than 0.5 cm in the plane transverse to it, and have a polar angle in the CDC acceptance range $[17^\circ, 150^\circ]$. These requirements reduce backgrounds with poorly reconstructed tracks and tracks from beam background.

Photon candidates are identified as localized energy deposits in the ECL not associated with any track. To suppress beam-induced photons, which have different energy

spectra depending on their momentum direction, each photon is required to have an energy greater than 30 MeV if reconstructed in the central region of the calorimeter, greater than 80 MeV if reconstructed in the backward region, and greater than 120 MeV if reconstructed in the forward region. Neutral pions are reconstructed from pairs of photon candidates that have an angular separation of less than 52° in the lab frame and an invariant mass in the range $[121 \text{ MeV}, 142 \text{ MeV}]$.

We reconstruct D mesons by combining two to four particles, one of them being identified as a K^+ . The mass of \bar{D}^0 candidates must be in the range $[1.845 \text{ MeV}, 1.885 \text{ MeV}]$ for $\bar{D}^0 \rightarrow K^+\pi^-$ and $\bar{D}^0 \rightarrow K^+\pi^-\pi^+\pi^-$, and in the range $[1.810 \text{ MeV}, 1.895 \text{ MeV}]$ for $\bar{D}^0 \rightarrow K^+\pi^-\pi^0$. The mass of D^- candidates is required to be in the range $[1.860 \text{ MeV}, 1.880 \text{ MeV}]$. The mass range is looser for \bar{D}^0 candidates, as the selection requirements placed on the D^{*-} are sufficient to suppress background events containing a fake \bar{D}^0 .

We identify negatively charged pions with momenta below 300 MeV in the center-of-mass frame as slow pion candidates. Each of these candidates is combined with a \bar{D}^0 candidate to form a D^{*-} candidate. The energy released in the D^{*-} decay, $m(D^{*-}) - m(\bar{D}^0) - m_{\pi^+}$, must be in the range $[4.6 \text{ MeV}, 7.0 \text{ MeV}]$.

Each $D^{(*)-}$ is combined with a remaining positive particle to form a B_{sig} candidate. To remove background from $B^0 \rightarrow D^{(*)-}\ell^+\nu_\ell$ decays, we require the particle to be identified as a pion. A small number of Cabibbo-suppressed $B^0 \rightarrow D^{(*)-}K^+$ decays pass this requirement. Their yield is 2.7% of that of $B^0 \rightarrow D^{(*)-}\pi^+$ decays. These decays have the same Δt distribution as $B^0 \rightarrow D^{(*)-}\pi^+$, and we treat them as signal.

We identify B_{sig} candidates using two quantities, the beam-constrained mass M_{bc} and the energy difference ΔE . These quantities are defined as

$$M_{\text{bc}} \equiv \sqrt{E_{\text{beam}}^2 - |\vec{p}|^2}, \quad \Delta E \equiv E - E_{\text{beam}}, \quad (2)$$

where E_{beam} is the beam energy, and \vec{p} and E are the reconstructed momentum and energy, respectively, of the B_{sig} candidate. All quantities are calculated in the e^+e^- center-of-mass frame. We calculate E assuming that the track directly from B_{sig} is a pion. We require that M_{bc} be greater than 5.27 GeV and that ΔE be in the range $[-0.10 \text{ GeV}, 0.25 \text{ GeV}]$. The ΔE range is asymmetric, *i.e.*, shorter on the lower side, to reduce backgrounds from B decays with missing daughters.

We determine the B_{tag} vertex and flavor using the remaining tracks in the event. Such tracks are required to have at least one hit in each of the PXD, SVD, and CDC and have a reconstructed momentum greater than 50 MeV. Each track must also originate from the e^+e^- interaction point according to the same criteria as used to select B_{sig} candidates. We require that the B_{tag} decay includes at least one charged particle. The B_{tag} momentum is taken to be opposite that of the B_{sig} candidate in

the center-of-mass frame.

To determine the B_{sig} decay vertex, we fit its decay chain with the `TreeFit` algorithm [31, 32]. To determine the B_{tag} decay vertex, we fit its decay products with the `Rave` adaptive algorithm [33], which accounts for our lack of knowledge of the decay chain by reducing the impact of tracks displaced by potential intermediate D decays. The decay vertex position is adjusted such that the direction of each B^0 , as determined from its decay vertex and the e^+e^- interaction point [34], is parallel to its momentum vector. The IR is measured from $e^+e^- \rightarrow \mu^+\mu^-$ events. Charged D candidates must have positive flight distances. We require that both vertex fits converge, and that the uncertainty on the decay time, $\sigma_{\Delta t_\ell}$, as calculated from the fitted vertex positions, be less than 2 ps. These vertex quality requirements retain approximately 90% of signal events.

The efficiency to reconstruct a $B_{\text{sig}}B_{\text{tag}}$ pair with $B_{\text{sig}} \rightarrow D^-\pi^+$ is 34%. For $B_{\text{sig}} \rightarrow D^{*-}\pi^+$ with $\bar{D}^0 \rightarrow K^+\pi^-$, it is 35%; with $\bar{D}^0 \rightarrow K^+\pi^-\pi^0$, it is 15%; and with $\bar{D}^0 \rightarrow K^+\pi^-\pi^+\pi^-$, it is 25%. In 2.2% of selected events, there is more than one B_{sig} candidate. We retain all such candidates for further analysis.

The main sources of background are misreconstructed $\Upsilon(4S) \rightarrow B\bar{B}$ events and nonresonant $e^+e^- \rightarrow q\bar{q}$ events. To distinguish between signal and $q\bar{q}$, we train two multivariate classifiers [35]: one for $B^0 \rightarrow D^-\pi^+$ decays and one for $B^0 \rightarrow D^{*-}\pi^+$ decays. The classifiers exploit the difference in event topologies and use as input the following quantities: Fox-Wolfram moments [36] and an extension thereof [37]; ‘‘cone’’ variables developed by the CLEO collaboration [38]; the angle between the thrust axes of the two B mesons [39]; and the event sphericity [40]. The classifiers are trained and tested using simulated data. In addition to determining the flavor of each B_{tag} , the flavor-tagging algorithms return a tag-quality variable r , which ranges from 0 for no flavor information to +1 for unambiguous flavor assignment. From the B_{tag} and B_{sig} flavors, we determine the relative flavor q_f . The data is divided into seven subsamples, depending on the r value: [0.0, 0.10], [0.10, 0.25], [0.25, 0.45], [0.45, 0.60], [0.60, 0.725], [0.725, 0.875], and [0.875, 1.0]. This division enhances the statistical precision of the Δm_d measurement.

We determine the signal yield by performing an unbinned, extended maximum-likelihood fit to the distributions of ΔE and the multivariate-classifier output C . The fit is performed separately for each r interval and determines the yield of signal events and $B\bar{B}$ and $q\bar{q}$ background events. As the fit observables ΔE and C are found to have negligible correlation, the PDFs (P) for these variables are taken to factorize: $P(\Delta E, C) = P(\Delta E) \cdot P(C)$. All PDFs are determined separately for each r interval; however, some of the parameters (as noted below) are taken to be common among the r intervals.

The ΔE PDF for signal is modeled as the sum of

two double-sided Crystal Ball functions [41]: one for $B^0 \rightarrow D^{(*)-}\pi^+$ decays and one for $B^0 \rightarrow D^{(*)-}K^+$ decays. The shape parameters of these functions, as well as the ratio between their normalizations, are fixed to values obtained from simulation. To account for differences between data and simulation, we introduce two additional free parameters: a shift of the mean values of the functions, and a scale factor for their widths. These parameters are taken to be common among the r intervals. The ΔE PDF for $B\bar{B}$ background is a fourth-order polynomial, and the ΔE PDF for $q\bar{q}$ background is an exponential function. All parameters of the polynomial are fixed to values obtained from simulation, while the slope of the exponential function is free to vary.

The C PDFs for signal and background are taken to be Johnson S_U functions [42]. The Johnson functions across different r intervals have independent mode, standard deviation, skewness, and kurtosis parameters, all determined from simulation. We introduce four free parameters to account for differences between data and simulation that are common across all r intervals: one offset for the modes and one scale for the widths for all $q\bar{q}$ -background distributions; and similarly one offset and one scale common to all signal and $B\bar{B}$ -background distributions.

We simultaneously fit to data in all seven r intervals. The fit has a total of 28 free parameters: three yields for each of the r intervals, six scale or shift factors, and the slope of the exponential function used for the ΔE PDF of the $q\bar{q}$ background. The distributions of ΔE and C summed over all r intervals, along with projections of the fit results, are shown in Fig. 1. The resulting yields are $33\,317 \pm 203$ signal events, 2814 ± 150 $B\bar{B}$ -background events, and 5594 ± 125 $q\bar{q}$ -background events.

Using `sWeights` [43, 44] computed with the per-candidate signal fractions obtained from the fit to ΔE and C , we statistically subtract background contributions to the Δt and $\sigma_{\Delta t_\ell}$ distributions. In this manner, we need not parametrize background distributions when fitting for τ_{B^0} and Δm_d .

We measure the lifetime τ_{B^0} and oscillation frequency Δm_d by fitting the background-subtracted Δt and $\sigma_{\Delta t_\ell}$ distributions. The probability density to observe both B_{sig} and B_{tag} decays is obtained from eq. (1) by including the probability for B_{tag} to decay and the probability of mistagging its flavor,

$$P(\Delta t, \bar{t}, q_f, r | \tau_{B^0}, \Delta m_d) = \frac{e^{-2\bar{t}/\tau_{B^0}}}{\tau_{B^0}^2} \times \{1 + q_f[1 - 2w(r)] \cos(\Delta m_d \Delta t)\}, \quad (3)$$

where \bar{t} is the average of the B_{sig} and B_{tag} proper decay times, and $w(r)$ is the probability of the B_{tag} flavor being incorrectly assigned. The latter is parametrized with a single value for each r interval and is assumed to be independent of the B_{tag} flavor.

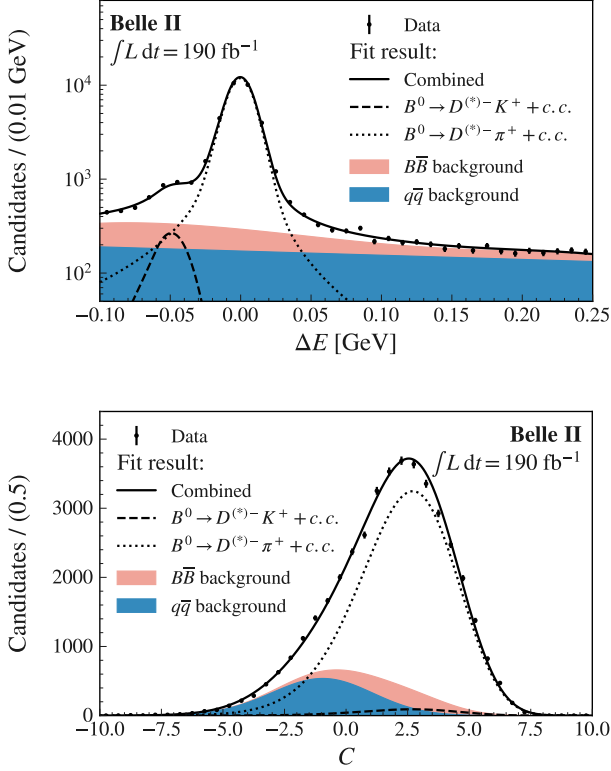


FIG. 1. Distributions of ΔE (top) and C (bottom) in data (points) and the fit model (curves and stacked shaded regions).

The decay-time difference Δt can be expressed as

$$\Delta t = \Delta t_\ell - 2 \frac{\beta_B}{\beta} \bar{t} \cos \theta, \quad (4)$$

where $\Delta t_\ell \equiv \ell / (\beta \gamma \gamma_B)$. In this expression, ℓ is the displacement of the B_{sig} vertex from that of B_{tag} , β is the velocity of the $\Upsilon(4S)$ in the lab frame (with $\gamma = (1 - \beta^2)^{-\frac{1}{2}}$), β_B is the velocity of a B in the $\Upsilon(4S)$ rest frame, and θ is the polar angle of the B_{sig} direction in the $\Upsilon(4S)$ rest frame. We integrate out the dependence of eq. (3) on \bar{t} and θ , accounting for the angular distribution in $e^+e^- \rightarrow \Upsilon(4S) \rightarrow B\bar{B}$, $P_\theta(\cos \theta) = (3/4)(1 - \cos^2 \theta)$.

To account for resolution and bias in measuring ℓ , we convolve eq. (3) with an empirical response function,

which is modeled as a linear combination of three components:

$$R(\delta t | \sigma_{\Delta t_\ell}) = (1 - f_t - f_{\text{OL}})G(\delta t | m_G \sigma_{\Delta t_\ell}, s_G \sigma_{\Delta t_\ell}) + f_t(\sigma_{\Delta t_\ell})R_t(\delta t | m_t \sigma_{\Delta t_\ell}, s_t \sigma_{\Delta t_\ell}, k / \sigma_{\Delta t_\ell}, f_>, f_<) + f_{\text{OL}}G(\delta t | 0, \sigma_0), \quad (5)$$

where $\delta t \equiv (\ell - \ell_{\text{true}}) / (\beta \gamma \gamma_B)$ and ℓ_{true} is the true value of ℓ . The first component is a Gaussian distribution with mean and standard deviation proportional to the per-candidate $\sigma_{\Delta t_\ell}$; this component accounts for 70% of candidates. The second component is a weighted sum of a Gaussian distribution and two exponentially modified Gaussian functions, corresponding to a Gaussian convolved with an exponential distribution,

$$R_t(x | \mu, \sigma, \kappa, f_<, f_>) = (1 - f_< - f_>)G(x | \mu, \sigma) + f_<G(x | \mu, \sigma) \otimes \kappa \exp_<(\kappa x) + f_>G(x | \mu, \sigma) \otimes \kappa \exp_>(-\kappa x), \quad (6)$$

where $\exp_>(-\kappa x) = \exp(-\kappa x)$ if $x > 0$ and $\exp_>(-\kappa x) = 0$ otherwise, and similarly for $\exp_<(\kappa x)$. The exponential tails account for poorly determined B_{tag} vertices due to intermediate charm mesons yielding displaced secondary vertices. The fraction f_t is zero at low values of $\sigma_{\Delta t_\ell}$ and reaches a plateau of 0.2 at approximately $\sigma_{\Delta t_\ell} = 25$ ps. This is modeled using three parameters: the maximal tail fraction f_t^{max} at its plateau, a threshold parameter describing the $\sigma_{\Delta t_\ell}$ value at which the tail fraction becomes nonzero, and a slope parameter describing how fast the tail fraction reaches its plateau. The third component has a large width, $\sigma_0 = 200$ ps, to account for the $\mathcal{O}(10^{-3})$ fraction of outlying poorly reconstructed vertices.

Equation (5) is the simplest model found to satisfactorily describe the δt distribution of simulated events. We fix σ_0 , as well as k , $f_>$, $f_<$, and the f_t slope and threshold parameters, to values determined from a fit to simulated data. Figure 2 shows the δt distribution of simulated data and the distribution of the fitted model. The parameter f_t^{max} , as well as the scaling factors relating the modes and standard deviations of G and R_t to $\sigma_{\Delta t_\ell}$ — m_G , s_G , m_t and s_t — are free to vary in the fit to data.

After integrating over $\cos \theta$ and \bar{t} and convolving with $R(\delta t)$, the Δt_ℓ distribution of B meson pairs is

$$P(\Delta t_\ell, \sigma_{\Delta t_\ell}, q_f, r | \tau_{B^0}, \Delta m_d) = P(\sigma_{\Delta t_\ell} | q_f, r) \int P(\Delta t - \delta t, \bar{t}, q_f, r | \tau_{B^0}, \Delta m_d) P_\theta(\cos \theta) R(\delta t | \sigma_{\Delta t_\ell}) d\delta t d\cos \theta d\bar{t}, \quad (7)$$

where $P(\sigma_{\Delta t_\ell} | q_f, r)$ is the probability to observe $\sigma_{\Delta t_\ell}$ for a given value of q_f and r , modelled using histogram templates: one for each r interval and value of q_f (14 in

total), taken from the data. The sWeights computed using the fit to ΔE and C are used to statistically subtract the background contribution to the $\sigma_{\Delta t_\ell}$ histograms. We

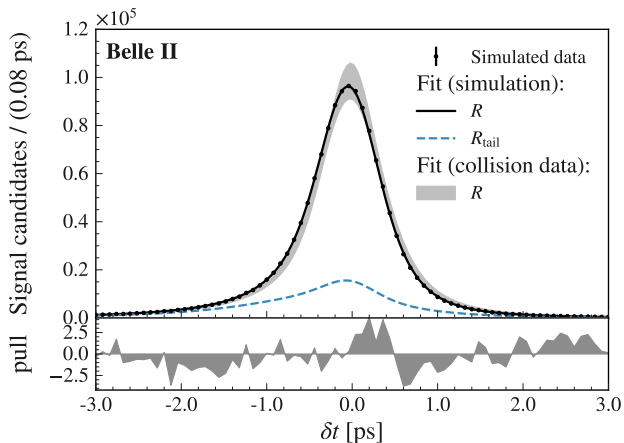


FIG. 2. Top: Distribution of δt in simulated data (points) and distribution modeled by the response function from the fit to the simulated data (curves) and from the fit to the experimental data (shaded). The shaded area accounts for the statistical and systematic uncertainties on the parameters of the response function. Bottom: distribution of the pull, defined as the difference between the event count in each bin and its value predicted by the fit, divided by the Poisson uncertainty.

fit for τ_{B^0} and Δm_d by maximizing

$$\sum_i s^i \ln P(\Delta t_\ell^i, \sigma_{\Delta t_\ell}^i, q_f^i, r^i | \tau_{B^0}, \Delta m_d), \quad (8)$$

where the sum runs over all $B_{\text{sig}} B_{\text{tag}}$ candidate pairs and s^i is the sWeight of a pair. Fourteen parameters are free in the fit: τ_{B^0} and Δm_d ; seven values of w , one for each r interval; and the five free parameters of the response function.

We calculate the statistical uncertainties using 1000 bootstrapped [45] samples obtained from the data. For each sample, we repeat the determination of the sWeights and the fit for τ_{B^0} and Δm_d . In this way, the spread of fitted τ_{B^0} and Δm_d values account for the statistical fluctuations of the signal and background fractions. We test this analysis method with independent simulated data. When tested on simulated data, our fitting procedure determines τ_{B^0} with a small systematic bias of (0.004 ± 0.002) ps and Δm_d with no significant bias, (0.000 ± 0.001) ps⁻¹. We assign the central value of the bias on τ_{B^0} as a systematic uncertainty. We assign the uncertainty on the bias on Δm_d , arising from the size of the simulated data, as a systematic uncertainty.

The Δt_ℓ distributions of both opposite-flavor and same-flavor B -meson pairs are shown in Fig. 3 for all r intervals combined, along with projections of the fit result. We also check that the fit quality is good in each individual r interval. The figure shows the Δt_ℓ -dependent yield asymmetry between the two samples, defined as the

difference between the number of opposite-flavor pairs and same-flavor pairs divided by their sum. The fit results and statistical uncertainties for τ_{B^0} and Δm_d are (1.499 ± 0.013) ps and (0.516 ± 0.008) ps⁻¹, with a -29% statistical correlation factor between them.

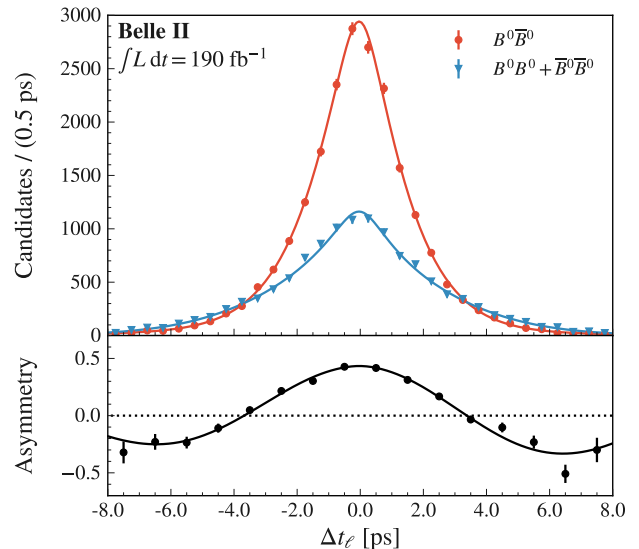


FIG. 3. Distribution of Δt_ℓ in data (points) and the fit model (lines) for opposite-flavor candidate pairs (red) and same-flavor pairs (blue) and their asymmetry (black).

There are several sources of systematic uncertainty; these are listed in Tab. I and described below. The dominant systematic uncertainty is due to potential discrepancies between the assumed values (fixed in the fit) of the response-function parameters and the true values in the data. For each fixed parameter, we repeat the fit with the parameter allowed to vary. We add all the resulting changes in the result in quadrature and include this value as a systematic uncertainty.

TABLE I. Systematic uncertainties.

Source	τ_{B^0} [ps]	Δm_d [ps ⁻¹]
Fixed response-function parameters	0.006	0.003
Analysis bias	0.004	0.001
Detector alignment	0.003	0.002
Interaction-region precision	0.002	0.001
C -Distribution modeling	0.000	0.001
$\sigma_{\Delta t_\ell}$ -Distribution modeling	0.001	0.001
Correlations of ΔE or C and Δt_ℓ	0.001	0.000
Total systematic uncertainty	0.008	0.005
Statistical uncertainty	0.013	0.008

Possible misalignment of the tracking detector can bias our results [46]. To estimate this effect, we reconstruct simulated signal events with several misalignment scenarios. Two scenarios are extracted from collision data using

day-by-day variations of the detector alignment. Two additional scenarios correspond to misalignments remaining after applying the alignment procedure to dedicated simulated data. We repeat the analysis for each scenario and assign the largest changes in the results as systematic uncertainties.

Because we adjust the B_{sig} decay vertex position so that the vector connecting the IR and decay vertex is parallel to the B_{sig} momentum, the precision to which we know the IR affects our determination of ℓ . We repeat our analysis on simulated data in which we shift, rotate, and rescale the IR within its measured uncertainties and assign the changes in the results as systematic uncertainties. We perform an analogous check with changes to \sqrt{s} and the magnitude and direction of the boost vector and find that the results change negligibly.

We estimate systematic uncertainties due to mismodeling the C distribution, including possible correlation with ΔE , from the changes in the results observed when fitting to the ΔE distribution only. In that case, the $B\bar{B}$ -background fraction is fixed to the value in simulated data. The result for τ_{B^0} changes negligibly, but a systematic uncertainty is included for Δm_d . To check for dependence of the results on the ΔE model for the $q\bar{q}$ and $B\bar{B}$ backgrounds, we repeat the analysis with each model replaced by a second-order polynomial with all parameters free in the fit. The polynomial parameters are common to all r intervals. The results change negligibly.

To check for dependence of the results on the $\sigma_{\Delta t_\ell}$ model, we repeat the fit with several alternative binning choices for their templates, and also replacing templates with analytical functions. We assign the largest changes in the results as systematic uncertainties.

We investigate the impact of fixing the yield of $B^0 \rightarrow D^{(*)-}K^+$ decays relative to $B^0 \rightarrow D^{(*)-}\pi^+$ by repeating the analysis with alternative choices of the $B^0 \rightarrow D^{(*)-}K^+$ fraction, corresponding to varying the branching fractions and relevant hadron identification efficiencies by their known uncertainties [47]. The results change negligibly.

To check if potential correlations of ΔE or C with Δt_ℓ affect our results, we repeat the analysis with sWeights calculated independently for two subgroups of candidate pairs, defined by the sign of Δt_ℓ . Likewise, we repeat the analysis for two subgroups defined by whether $|\Delta t_\ell|$ is greater or less than 1.150 ps. In both cases, the results change mildly and we assign the larger of these two changes as systematic uncertainties.

The global momentum scale of the Belle II tracking detector is calibrated to a relative precision of better than 0.1%, and the global length scale to a precision of better than 0.01%. Neither significantly impacts our results.

We further check our analysis by repeating it on subsets of the data divided by data-taking period or by whether the charm meson in the B_{sig} decay is D^- or D^{*-} . The results are all statistically consistent with each other and with our overall results.

In summary, we measure the B^0 lifetime and flavor-oscillation frequency using $B^0 \rightarrow D^{(*)-}\pi^+$ decays reconstructed in data collected from e^+e^- collisions at the $\Upsilon(4S)$ resonance and corresponding to an integrated luminosity of 190 fb^{-1} . The results are

$$\tau_{B^0} = (1.499 \pm 0.013 \pm 0.008) \text{ ps} \quad (9)$$

$$\Delta m_d = (0.516 \pm 0.008 \pm 0.005) \text{ ps}^{-1}. \quad (10)$$

The results agree with previous measurements and have very similar systematic uncertainties as compared to results from the Belle and Babar collaborations [3, 4]. They demonstrate a good understanding of the Belle II detector and provide a strong foundation for future time-dependent measurements.

ACKNOWLEDGMENTS

This work, based on data collected using the Belle II detector, which was built and commissioned prior to March 2019, was supported by Science Committee of the Republic of Armenia Grant No. 20TTCG-1C010; Australian Research Council and research Grants No. DE220100462, No. DP180102629, No. DP170102389, No. DP170102204, No. DP150103061, No. FT130100303, No. FT130100018, and No. FT120100745; Austrian Federal Ministry of Education, Science and Research, Austrian Science Fund No. P 31361-N36 and No. J4625-N, and Horizon 2020 ERC Starting Grant No. 947006 “InterLeptons”; Natural Sciences and Engineering Research Council of Canada, Compute Canada and CANARIE; Chinese Academy of Sciences and research Grant No. QYZDJ-SSW-SLH011, National Natural Science Foundation of China and research Grants No. 11521505, No. 11575017, No. 11675166, No. 11761141009, No. 11705209, and No. 11975076, Liaoning Revitalization Talents Program under Contract No. XLYC1807135, Shanghai Pujiang Program under Grant No. 18PJ1401000, Shandong Provincial Natural Science Foundation Project ZR2022JQ02, and the CAS Center for Excellence in Particle Physics (CCEPP); the Ministry of Education, Youth, and Sports of the Czech Republic under Contract No. LTT17020 and Charles University Grant No. SVV 260448 and the Czech Science Foundation Grant No. 22-18469S; European Research Council, Seventh Framework PEF-GA-2013-622527, Horizon 2020 ERC-Advanced Grants No. 267104 and No. 884719, Horizon 2020 ERC-Consolidator Grant No. 819127, Horizon 2020 Marie Skłodowska-Curie Grant Agreement No. 700525 “NIOBE” and No. 101026516, and Horizon 2020 Marie Skłodowska-Curie RISE project JENNIFER2 Grant Agreement No. 822070 (European grants); L’Institut National de Physique Nucléaire et de Physique des Particules (IN2P3) du CNRS (France); BMBF, DFG, HGF, MPG, and AvH Foundation (Germany); Department of Atomic Energy under Project Identification No. RTI 4002 and Department of Science

and Technology (India); Israel Science Foundation Grant No. 2476/17, U.S.-Israel Binational Science Foundation Grant No. 2016113, and Israel Ministry of Science Grant No. 3-16543; Istituto Nazionale di Fisica Nucleare and the research grants BELLE2; Japan Society for the Promotion of Science, Grant-in-Aid for Scientific Research Grants No. 16H03968, No. 16H03993, No. 16H06492, No. 16K05323, No. 17H01133, No. 17H05405, No. 18K03621, No. 18H03710, No. 18H05226, No. 19H00682, No. 22H00144, No. 26220706, and No. 26400255, the National Institute of Informatics, and Science Information NETWORK 5 (SINET5), and the Ministry of Education, Culture, Sports, Science, and Technology (MEXT) of Japan; National Research Foundation (NRF) of Korea Grants No. 2016R1D1A1B-02012900, No. 2018R1A2B3003643, No. 2018R1A6A1A-06024970, No. 2018R1D1A1B07047294, No. 2019R1-I1A3A01058933, No. 2022R1A2C1003993, and No. RS-2022-00197659, Radiation Science Research Institute, Foreign Large-size Research Facility Application Supporting project, the Global Science Experimental Data Hub Center of the Korea Institute of Science and Technology Information and KREONET/GLORIAD; Universiti Malaya RU grant, Akademi Sains Malaysia, and Ministry of Education Malaysia; Frontiers of Science Program Contracts No. FOINS-296, No. CB-221329, No. CB-236394, No. CB-254409, and No. CB-180023, and No. SEP-CINVESTAV research Grant No. 237 (Mexico); the Polish Ministry of Science and Higher Education and the National Science Center; the Ministry of Science and Higher Education of the Russian Federation, Agreement No. 14.W03.31.0026, and the HSE University Basic Research Program, Moscow; University of Tabuk research Grants No. S-0256-1438 and No. S-0280-1439

(Saudi Arabia); Slovenian Research Agency and research Grants No. J1-9124 and No. P1-0135; Agencia Estatal de Investigacion, Spain Grant No. RYC2020-029875-I and Generalitat Valenciana, Spain Grant No. CIDE-GENT/2018/020 Ministry of Science and Technology and research Grants No. MOST106-2112-M-002-005-MY3 and No. MOST107-2119-M-002-035-MY3, and the Ministry of Education (Taiwan); Thailand Center of Excellence in Physics; TUBITAK ULAKBIM (Turkey); National Research Foundation of Ukraine, project No. 2020.02/0257, and Ministry of Education and Science of Ukraine; the U.S. National Science Foundation and research Grants No. PHY-1913789 and No. PHY-2111604, and the U.S. Department of Energy and research Awards No. DE-AC06-76RLO1830, No. DE-SC0007983, No. DE-SC0009824, No. DE-SC0009973, No. DE-SC0010007, No. DE-SC0010073, No. DE-SC0010118, No. DE-SC0010504, No. DE-SC0011784, No. DE-SC0012704, No. DE-SC0019230, No. DE-SC0021274, No. DE-SC0022350; and the Vietnam Academy of Science and Technology (VAST) under Grant No. DL0000.05/21-23.

These acknowledgements are not to be interpreted as an endorsement of any statement made by any of our institutes, funding agencies, governments, or their representatives.

We thank the SuperKEKB team for delivering high-luminosity collisions; the KEK cryogenics group for the efficient operation of the detector solenoid magnet; the KEK computer group and the NII for on-site computing support and SINET6 network support; and the raw-data centers at BNL, DESY, GridKa, IN2P3, INFN, and the University of Victoria for offsite computing support.

-
- [1] A. Lenz, *Int. J. Mod. Phys. A* **30**, 1543005 (2015), arXiv:1405.3601 [hep-ph].
- [2] R. J. Dowdall, C. T. H. Davies, R. R. Horgan, G. P. Lepage, C. J. Monahan, J. Shigemitsu, and M. Wingate, *Phys. Rev. D* **100**, 094508 (2019), arXiv:1907.01025 [hep-lat].
- [3] K. Abe *et al.* (Belle Collaboration), *Phys. Rev. D* **71**, 072003 (2005), arXiv:hep-ex/0408111.
- [4] B. Aubert *et al.* (Babar Collaboration), *Phys. Rev. D* **73**, 012004 (2006), arXiv:hep-ex/0507054.
- [5] R. Aaij *et al.* (LHCb Collaboration), *JHEP* **04**, 114, arXiv:1402.2554 [hep-ex].
- [6] R. Aaij *et al.* (LHCb Collaboration), *Eur. Phys. J. C* **76**, 412 (2016), arXiv:1604.03475 [hep-ex].
- [7] A. M. Sirunyan *et al.* (CMS Collaboration), *Eur. Phys. J. C* **78**, 457 (2018), arXiv:1710.08949 [hep-ex].
- [8] G. Aad *et al.* (ATLAS Collaboration), *Phys. Rev. D* **87**, 032002 (2013), arXiv:1207.2284 [hep-ex].
- [9] V. M. Abazov *et al.* (D0 Collaboration), *Phys. Rev. Lett.* **114**, 062001 (2015), arXiv:1410.1568 [hep-ex].
- [10] T. Aaltonen *et al.* (CDF Collaboration), *Phys. Rev. Lett.* **106**, 121804 (2011), arXiv:1012.3138 [hep-ex].
- [11] We use a system of units in which $\hbar = c = 1$ and mass and frequency have the same dimension.
- [12] Another naming convention, with $\beta \equiv \phi_1$ and $\alpha \equiv \phi_2$, is also used in the literature.
- [13] I. Adachi *et al.* (Belle Collaboration), *Phys. Rev. Lett.* **108**, 171802 (2012), arXiv:1201.4643 [hep-ex].
- [14] P. Vanhoefer *et al.* (Belle Collaboration), *Phys. Rev. D* **93**, 032010 (2016), [Addendum: *Phys.Rev.D* 94, 099903 (2016)], arXiv:1510.01245 [hep-ex].
- [15] M. Beneke, G. Buchalla, M. Neubert, and C. T. Sachrajda, *Nucl. Phys. B* **591**, 313 (2000), arXiv:hep-ph/0006124.
- [16] R. Aaij *et al.* (LHCb Collaboration), *JHEP* **06**, 084, arXiv:1805.03448 [hep-ex].
- [17] B. Aubert *et al.* (Babar Collaboration), *Phys. Rev. D* **73**, 111101 (2006), arXiv:hep-ex/0602049.
- [18] S. Bahinipati *et al.* (Belle Collaboration), *Phys. Rev. D* **84**, 021101 (2011), arXiv:1102.0888 [hep-ex].
- [19] F. Abudinén *et al.* (Belle II Collaboration), *Eur. Phys. J. C* **82**, 283 (2022), Here we use the category-based algorithm, arXiv:2110.00790 [hep-ex].
- [20] I. I. Y. Bigi and A. I. Sanda, *Nucl. Phys. B* **193**, 85

- (1981).
- [21] P. Oddone, *UCLA Linear-Collider BB Factory Concep. Design: Proceedings*, eConf **C870126**, 423 (1987).
- [22] K. Akai, K. Furukawa, and H. Koiso (SuperKEKB), *Nucl. Instrum. Meth. A* **907**, 188 (2018), arXiv:1809.01958 [physics.acc-ph].
- [23] T. Abe *et al.* (Belle II Collaboration), (2010), arXiv:1011.0352 [physics.ins-det].
- [24] T. Kuhr, C. Pulvermacher, M. Ritter, T. Hauth, and N. Braun (Belle II Framework Software Group), *Comput. Softw. Big Sci.* **3**, 1 (2019), arXiv:1809.04299 [physics.comp-ph].
- [25] V. Bertacchi *et al.* (Belle II Tracking Group), *Comput. Phys. Commun.* **259**, 107610 (2021), arXiv:2003.12466 [physics.ins-det].
- [26] S. Jadach, B. F. L. Ward, and Z. Was, *Comput. Phys. Commun.* **130**, 260 (2000), arXiv:hep-ph/9912214.
- [27] T. Sjöstrand, S. Ask, J. R. Christiansen, R. Corke, N. Desai, P. Ilten, S. Mrenna, S. Prestel, C. O. Rasmussen, and P. Z. Skands, *Comput. Phys. Commun.* **191**, 159 (2015), arXiv:1410.3012 [hep-ph].
- [28] D. J. Lange, *Nucl. Instrum. Meth. A* **462**, 152 (2001).
- [29] S. Agostinelli *et al.* (GEANT4 software Group), *Nucl. Instrum. Meth. A* **506**, 250 (2003).
- [30] Z. J. Liptak *et al.*, *Nucl. Instrum. Meth. A* **1040**, 167168 (2022), arXiv:2112.14537 [physics.ins-det].
- [31] W. Hulsbergen, *Nucl. Instrum. Meth. A* **600**, 471 (2009), arXiv:0810.2241 [physics.ins-det].
- [32] J. F. Krohn *et al.* (Belle II analysis software Group), *Nucl. Instrum. Meth. A* **976**, 164269 (2020), arXiv:1901.11198 [hep-ex].
- [33] W. Waltenberger, W. Mitaroff, F. Moser, B. Pflugfelder, and H. V. Riedel, *J. Phys. Conf. Ser.* **119**, 032037 (2008).
- [34] S. Dey and A. Soffer, *Springer Proc. Phys.* **248**, 411 (2020).
- [35] T. Chen and C. Guestrin, in *Proceedings of the 22nd ACM SIGKDD International Conference on Knowledge Discovery and Data Mining, KDD '16* (Association for Computing Machinery, New York, NY, USA, 2016) p. 785–794.
- [36] G. C. Fox and S. Wolfram, *Phys. Rev. Lett.* **41**, 1581 (1978).
- [37] S. H. Lee *et al.* (Belle Collaboration), *Phys. Rev. Lett.* **91**, 261801 (2003), arXiv:hep-ex/0308040.
- [38] D. M. Asner *et al.* (CLEO Collaboration), *Phys. Rev. D* **53**, 1039 (1996), arXiv:hep-ex/9508004.
- [39] Ed. A.J. Bevan, B. Golob, Th. Mannel, S. Prell, and B.D. Yabsley, *Eur. Phys. J. C* **74**, 3026 (2014), Chapter 9, arXiv:1406.6311 [hep-ex].
- [40] G. Parisi, *Phys. Lett. B* **74**, 65 (1978).
- [41] T. Skwarnicki, *A study of the radiative CASCADE transitions between the Upsilon-Prime and Upsilon resonances*, Ph.D. thesis, Cracow, INP (1986).
- [42] N. L. Johnson, *Biometrika* **36**, 149 (1949).
- [43] M. Pivk and F. R. Le Diberder, *Nucl. Instrum. Meth. A* **555**, 356 (2005), arXiv:physics/0402083.
- [44] H. Dembinski, M. Kenzie, C. Langenbruch, and M. Schmelling, (2021), arXiv:2112.04574 [stat.ME].
- [45] B. Efron, *The Annals of Statistics* **7**, 1 (1979).
- [46] T. Bilka, J. Kandra, C. Kleinwort, and R. Zlebcik, *EPJ Web Conf.* **251**, 03028 (2021).
- [47] R. L. Workman *et al.* (Particle Data Group), *PTEP* **2022**, 083C01 (2022).